Title

High resolution in vivo characterization of apparent diffusion coefficient at the tumor–stromal boundary of breast carcinomas: A pilot study to assess treatment response using proximity-dependent diffusion-weighted imaging

Journal

Journal of Magnetic Resonance Imaging, 39(5)

ISSN

1053-1807

Authors

McLaughlin, Rebekah L
Newitt, David C
Wilmes, Lisa J
et al.

Publication Date

2014-05-01

DOI

10.1002/jmri.24283

Peer reviewed

Published in final edited form as:
J Magn Reson Imaging. 2014 May ; 39(5): 1308–1313. doi:10.1002/jmri.24283.

High Resolution *In Vivo* Characterization of Apparent Diffusion Coefficient at the Tumor-Stromal Boundary of Breast Carcinomas: A Pilot Study to Assess Treatment Response Using Proximity-Dependent Diffusion-Weighted Imaging

Rebekah L. McLaughlin, MPhil[1,2], **David C. Newitt, PhD**[2], **Lisa J. Wilmes, PhD**[2], **Ella F. Jones, PhD**[2], **Dorota J. Wisner, MD, PhD**[2], **John Kornak, PhD**[3], **Evelyn Proctor, BS**[2], **Bonnie N. Joe, MD, PhD**[2], and **Nola M. Hylton, PhD**[1,2]

[1]The UC Berkeley - UCSF Graduate Program in Bioengineering, San Francisco and Berkeley, California

[2]Department of Radiology and Biomedical Imaging, UCSF, San Francisco, California

[3]Department of Epidemiology and Biostatistics, UCSF, San Francisco, California

Abstract

Purpose—To evaluate diffusion changes in the breast tumor-stromal boundary and adjacent tissue in response to neoadjuvant chemotherapy using high resolution diffusion-weighted imaging (HR-DWI).

Materials and Methods—Seven patients with invasive breast cancer were imaged with HR-DWI before and early during treatment. The mean apparent diffusion coefficient (ADC) was plotted in 1 mm increments around the tumor boundary. Early change in ADC was measured for tumor, tumor boundary, and stromal regions, and the relationship to treatment response was evaluated using Spearman's correlation.

Results—Statistically significant correlations between treatment response and early changes in ADC were found for: 1) whole tumor ($\rho = 0.93$, 95% CI = (0.58, 0.99), $p = 0.003$); 2) tumor rim ($\rho = 0.75$, 95% CI = (−0.007, 0.96), $p = 0.05$); and 3) boundary transition region ($\rho = 0.86$, 95% CI = (0.29, 0.98), $p = 0.01$). Early change in ADC of distal stroma had a marginally statistically significant positive correlation to treatment response ($\rho = 0.71$, 95% CI = (−0.084, 0.95), $p = 0.07$).

Conclusion—Proximity-dependent evaluation of HR-DWI data in the breast tumor-stromal boundary and adjacent tissue may provide information about response to therapy.

Keywords

breast cancer; neoadjuvant chemotherapy; MRI; DWI

INTRODUCTION

The tumor microenvironment is known to play a role in tumorigenesis (1–3). The architecture of the extracellular matrix (ECM) at the breast tumor-stroma border may facilitate local and metastatic invasion (4–7). ECM remodeling alters stromal properties by

Corresponding Author and Reprint Info: Nola Hylton, University of California, San Francisco, 1600 Divisadero Street, C250, Box 1667, San Francisco, CA 94115, Phone: (415) 885-7511, Fax: (415) 885-3884, nola.hylton@ucsf.edu.

altering matrix cross-linking, increasing collagen deposition, and reorganizing fibers, leading to an increase in tissue stiffness (8). Although several imaging techniques have been developed to characterize the progressive stiffening of cancer tissue *in vivo* (9–11), research continues to rely primarily on *ex vivo* biopsy or surgical samples and representative cell lines grown *in vitro*.

Apparent diffusion coefficient (ADC) is a measure of water mobility in diffusion-weighted imaging (DWI). It uses diffusion sensitizing gradients to detect changes in water movement. Decreased ADC relative to normal breast tissue has been shown to be associated with malignant lesions (12, 13). However, standard DWI using echo planar imaging (EPI) methods has been limited by low signal-to-noise and image distortion. Recently reported results implemented a high-resolution diffusion-weighted imaging (HR-DWI) acquisition to gain a substantial increase in resolution with decreased distortion in breast tumor characterization (14).

For this pilot study, we hypothesized that HR-DWI may be sensitive to water mobility changes associated with ECM remodeling at the tumor-stroma border, as well as changes in these microstructures in response to treatment. The objective of this study was to use proximity-dependent evaluation of HR-DWI to characterize the diffusion behavior of the breast tumor-stromal boundary and adjacent tissue in patients receiving neoadjuvant treatment. Here we present the initial findings of ADC changes in the tumor-stroma environment and their association with treatment response.

MATERIALS AND METHODS

Study Population

Seven patients with pathological confirmed invasive breast cancer who underwent neoadjuvant chemotherapy using taxane-based treatment followed by doxorubicin cyclophosphamide (AC) were evaluated with dynamic contrast-enhanced magnetic resonance imaging (DCE MRI) and HR-DWI. All patients signed informed consent. MRI scans were performed before treatment (V1); early in the course of taxane-based treatment (V2); after completion of taxane-based and before AC treatment (V3) and after the completion of all chemotherapy (V4).

MRI Acquisition

MRI data were collected on a 1.5 T GE Signa LX scanner (GE Healthcare, Milwaukee, WI) using a bilateral 8-channel phased array coil (Hologic - formerly Sentinelle Medical, Toronto, Canada). A bilateral fat-suppressed T1-weighted DCE MRI was acquired with a three-dimensional fast gradient echo sequence. The DCE MRI scan time was between 80–100 sec per phase, and scan collection continued for at least 8 min following contrast injection. Patients received 0.1 mmol/kg body weight of gadopentetate dimeglumine (Magnevist, Bayer Healthcare Pharmaceuticals, Berlin, Germany) contrast agent. In addition to DCE MRI, HR-DWI data (15) were acquired with an echo planar imaging sequence and the following parameters: repetition time (TR), 4000 ms; echo time (TE), 64.8 ms; field of view (FOV), 140 × 70 mm; acquisition matrix, 128 × 64; in-plane resolution, 1.094 × 1.094 mm; slice thickness, 4 mm. Either 8 or 16 slices were acquired. Diffusion-weighting gradients were applied sequentially in three orthogonal directions with $b = 600$ s/mm^2. Images were also acquired with $b = 0$ s/mm^2.

MRI Analysis

Apparent diffusion coefficient (ADC) maps were created from complex averaged images using a method described previously (15). Briefly, after phase correction of the single-shot

k-space data, all the repetitions were complex averaged. Refocusing reconstruction was then applied to remove motion artifacts, followed by homodyne reconstruction to produce the final diffusion-weighted image. The ADC maps were calculated on a pixel-by-pixel basis, according to the equation: $ADC = -\ln[(S_D/S_0)/\Delta b]$, where S_0 and S_D are the signals at b = 0 s/mm^2 and b = 600 s/mm^2 respectively and Δb = 600 s/mm^2. The ADC images were manually segmented into enhancing tumor and surrounding stromal tissue. The tumor region of interest (ROI) was selected in all slices of the ADC map (Figure 1a), including regions that were assigned as partial volume averaged tumor based on consultation with a breast radiologist to interpret the DCE MRI and HR-DWI data.

All visible breast tissue was selected in a second set of ROIs on the b = 0 image of the HR-DWI, excluding the fat from the skin and any obvious artifacts from biopsy clips in the tumor. A fuzzy C-means clustering procedure was performed to select all fibroglandular tissue (16) visible on the HR-DWI (Figure 1b).

A proximity mapping method assigned each fibroglandular voxel a distance to the nearest tumor boundary voxel, assigning negative values to voxels within the tumor (17). This study calculated distances for each voxel relative only to the other voxels in the same slice and analyzed the results of every slice. The fibroglandular proximity map (Figure 1c) can be applied to any registered functional image to calculate proximity-dependent values; in this study, it was combined with the ADC map (Figure 1d). The mean ADC was calculated for the voxels in 1 mm thick concentric shells, starting at 10 mm inside the tumor (−10 mm) and ending at 20 mm away from the tumor edge.

The mean ADC for each shell was plotted as a function of distance from the tumor boundary for each patient at V1 and V2. In order to compare tumor to surrounding stroma, three regions were defined as shown in Figure 2: an inner section of tumor (−5 to −2 mm), a proximal stromal shell just outside the tumor (2 to 5 mm), and a distal stromal shell (9 to 13 mm). The mean ADC of all voxels in these regions were calculated and labeled ADC_{inner}, ADC_{prox}, and ADC_{dist}, respectively. The Wilcoxon signed rank test was used to compare ADC_{inner} to ADC_{prox} and ADC_{dist} at V1 and V2 for all patients. The same test was used to analyze the change in ADC_{inner}, ADC_{prox}, and ADC_{dist} from V1 to V2. Results are reported as (pseudo) medians, 95% confidence intervals (CI), and associated p-values. We consider a statistical significance level of $\alpha = 0.05$.

To compare tumor ADCs to the literature, $ADC_{wholetumor}$ was calculated for all voxels within the tumor boundary ($-\infty$ to 0 mm). To investigate the tumor boundary, ADC_{bound} was calculated for the boundary region of the tumor (−2 to 2 mm). Hereafter, ADC terms will be used to indicate the mean ADC of all voxels in the specified region, whereas mean ADC will refer to the mean of the specified ADC in the seven patients.

Treatment Response Assessment

For the purposes of this study, we defined treatment response as the percent decrease in a functional tumor volume from V1 to V4 measured by DCE MRI. The MR functional tumor volumes were calculated by applying a 70% contrast enhanced threshold to the DCE MRI data (18).

Spearman's rank correlation was used to estimate the strength of relationships between treatment response and each of the ADC measures. Results are reported as estimated correlations, 95% confidence intervals (CI) for the correlation, and associated p-values for rejecting the null hypothesis of zero correlation between treatment response and ADC. We consider a statistical significance level of $\alpha = 0.05$.

RESULTS

Patient Characteristics

Seven patients were included in this study with ages ranging from 38 to 58 (mean 50). The initial MR functional tumor volume ranged from 5.1 to 82.7 cm^3 (mean 36.0 cm^3). Treatment response, ie percent decrease in MR functional tumor volume, ranged from 30% to 98%.

Tumor-Stromal ADC Measurements

The ADC measurements from inner tumor to proximal and distal stromal regions in all seven patients displayed a consistent pattern. The inner tumor ADC values were lower than the surrounding proximal and distal stromal regions. There was an elevation of ADC to higher values at the boundary from −2 to 2 mm, followed by a plateau in the stroma. Figure 2a and 2b show example patterns of ADC values plotted against the distance from the tumor boundary from two patients at V1. Figure 2c illustrates the regions of ADC_{inner} (green), ADC_{prox} (blue), and ADC_{dist} (red) values extracted from the stromal proximity map overlaid on the ADC map.

Tumor-Stromal ADC Measurements Before Treatment (V1)

The units of the estimated (pseudo) medians and 95% CI for all ADC values are $\times 10^{-3}$ mm^2/s (results below are reported without units for brevity). Table 1 lists the ADC_{inner}, ADC_{prox}, ADC_{dist}, and $ADC_{wholetumor}$ values for all patients at V1 and V2. For all the patients at V1, the ADC_{inner} value was lower than both the ADC_{prox} and ADC_{dist} values. ADC_{inner} was lower than ADC_{prox} (estimated (pseudo) median difference = 0.59, 95% CI = (0.34, 0.95), p = 0.02), and ADC_{inner} was lower than ADC_{dist} (estimate = 0.61, 95% CI = (0.29, 0.92), p = 0.02). The ADC values were similar in ADC_{prox} and ADC_{dist} (estimated difference = −0.0097, 95% CI = (−0.13, 0.094), p = 0.94).

Tumor-Stromal ADC Measurements Early During Treatment (V2)

Early in the course of taxane-based treatment, the ADC_{inner} value in all patients had increased compared to V1 (estimated change = 0.19, 95% CI = (0.041, 0.38), p = 0.02). The ADC_{inner} value at V2 was lower than both the ADC_{prox} and ADC_{dist} values in all but one patient (Table 1). After early treatment, ADC_{inner} was lower than ADC_{prox} (estimated increase = 0.44, 95% CI = (0.16, 0.77), p = 0.03), and ADC_{inner} was also lower than ADC_{dist} (estimate = 0.38, 95% CI = (0.16, 0.72), p = 0.03). ADC_{prox} and ADC_{dist} were not statistically significantly different in value (estimated change = −0.0045, 95% CI = (−0.12, 0.058), p = 0.81). Unlike ADC_{inner}, our results showed no clear change in ADC_{prox} from V1 to V2 (estimated change = 0.024, 95% CI = (−0.097, 0.15), p = 0.81) nor in ADC_{dist} from V1 to V2 (estimated change = 0.019, 95% CI = (−0.087, 0.13), p = 0.69).

MR Functional Tumor Volumes

Early percent change in MR functional tumor volume, V1 to V2, showed no clear relationship with overall treatment response, V1 to V4 (Spearman $\rho = -0.36$, 95% CI = (−0.87, 0.54), p = 0.43). However, the confidence interval is wide, and we therefore cannot conclude a negative result with this limited dataset.

Association of ADC Measurements and Treatment Response

The Spearman's rank correlation between ADC measurements and treatment response are given in Table 2. As shown in Figure 3, early increases in ADC_{inner}, ADC_{bound}, and $ADC_{wholetumor}$ demonstrated a consistent pattern of correlation with increased treatment response. There was a statistically significant positive correlation between treatment

response and early change in ADC_{inner}; $\rho = 0.75$, 95% CI = (−0.007, 0.96), $p = 0.05$; early change in $ADC_{wholetumor}$: $\rho = 0.93$, 95% CI = (0.58, 0.99), $p = 0.003$; and early change in ADC_{bound}: $\rho = 0.86$, 95% CI = (0.29, 0.98), $p = 0.01$. There was an estimated positive correlation between treatment response and early change in ADC_{dist}: $\rho = 0.71$, 95% CI = (−0.084, 0.95), $p = 0.07$, though this was only marginally statistically significant. The early change in ADC_{prox} showed no clear relationship with treatment response, but we cannot conclude a negative result due to lack of statistical power (n = 7) and a wide confidence interval.

DISCUSSION

Using proximity-dependent HR-DWI measurements to characterize the primary tumor's diffusion behavior in patients receiving neoadjuvant treatment, we found statistically significant correlations between treatment response and early change in ADC_{inner} and $ADC_{wholetumor}$. These results agree with previous findings that tumor ADC increased as patients responded to neoadjuvant chemotherapy (13, 19).

We hypothesized that ECM collagen re-organization at the breast tumor-stroma border linked to tumor invasive potentials (4–7) and disease-free survival (20) may induce changes in diffusion behavior. Thus, our objective was to investigate whether ADC changes in the breast tumor-stromal boundary and adjacent tissue may indicate treatment response. Interestingly, treatment response correlated significantly with early change in ADC_{bound} and had a marginally statistically significant correlation to early change in ADC_{dist} - a stromal ADC measurement - which seems to support our hypothesis. The ADC_{dist} region was chosen to represent a region of normal-appearing stromal tissue; a region of tissue ~25 mm away from the tumor boundary showed a similar Spearman ρ and p value ($p = 0.05$).

This study was limited by a small sample size, and these results, while promising, require further validation with additional patients. Furthermore, MR functional tumor volume change was used to define treatment response in lieu of clinically accepted markers of response such as pathological complete response (pCR). MR functional tumor volume change provides a numerical scale of treatment response rather than a dichotomy of responders and non-responders like pCR, making it a more powerful evaluation of statistical correlations in a small sample population like this one.

Perhaps the largest challenge presented by the DWI data is the manual definition of the tumor boundary, which is both time-consuming and subjective. The tumor boundary was selected on each slice of the ADC map by the stark delineation between the dark and light voxels, as well as by referencing the $b = 0$ s/mm^2 image and combined $b = 600$ s/mm^2 image, both of which were co-localized and provided a clearer depiction of the encompassed anatomy. In addition, the DCE MRI images were referenced for a higher anatomical resolution image, with special attention paid to the enhancing volumes. Despite our efforts to minimize the variation in tumor boundary definition, we recognize that the boundary we defined was subjective. In order to mitigate errors induced by imprecise specification of the boundary, we defined the boundary as a ~4 mm wide strip (the region from −2 mm to 2 mm of the estimated boundary edge) for analysis purposes.

The use of a HR-DWI breast sequence allowed us to group the in-plane tumor and stroma tissue, as well as measure changes in diffusion within small distance ranges. Due to the large anisotropy of the HR-DWI voxels in this study, we chose to base our proximity calculations on within-plane data only. This definition of proximity for a voxel is solely determined within the same slice, and therefore proximity to tumor ignores any tumor voxels close by but in an adjacent slice. We are currently working to use a more isotropic voxel resolution

with the HR-DWI sequence, thereby increasing the utility of a true 3D proximity mapping method.

In conclusion, this proximity-dependent analysis of ADC shows promising results despite being limited by several technical challenges in data acquisition and analysis, a small sample size, and a lack of clinical endpoints. This new technique is a potentially useful tool for characterizing the breast tumor-stromal boundary and adjacent tissue, and our results suggest that stromal ADC measurements may provide information in addition tumor ADC and may correlate to treatment response. This work is ongoing, and we are gathering a larger data set to further investigate the nature of diffusion correlations to treatment response, including the addition of histopathological measures of treatment response.

Acknowledgments

Grant Support: This work was funded by Komen Grant SAC 110017, R01 CA69587, R01 116182, University of California Cancer Research Coordinating Committee (CRCC) Fellowship and National Institute of Health Training Grant GM008155-25.

References

1. Bissell MJ, Radisky DC, Rizki A, Weaver VM, Petersen OW. The organizing principle: Microenvironmental influences in the normal and malignant breast. Differentiation. 2002; 70:537–546. [PubMed: 12492495]
2. Polyak K, Kalluri R. The role of the microenvironment in mammary gland development and cancer. Cold Spring Harb Perspect Biol. 2010; 2:a003244. [PubMed: 20591988]
3. Tlsty TD, Coussens LM. Tumor stroma and regulation of cancer development. Annu Rev Pathol-Mech. 2006; 1:119–150.
4. Provenzano P, Eliceiri K, Campbell J, Inman D, White J, Keely P. Collagen reorganization at the tumor-stromal interface facilitates local invasion. BMC Med. 2006; 4:38. [PubMed: 17190588]
5. Provenzano PP, Inman DR, Eliceiri KW, Trier SM, Keely PJ. Contact guidance mediated three-dimensional cell migration is regulated by Rho/ROCK-dependent matrix reorganization. Biophys J. 2008; 95:5374–5384. [PubMed: 18775961]
6. Lopez JI, Kang I, You W-K, McDonald DM, Weaver VM. In situ force mapping of mammary gland transformation. Integr Biol. 2011; 3:910–921.
7. Provenzano P, Inman D, Eliceiri K, et al. Collagen density promotes mammary tumor initiation and progression. BMC Med. 2008; 6:11. [PubMed: 18442412]
8. Paszek MJ, Boettiger D, Weaver VM, Hammer DA. Integrin clustering is driven by mechanical resistance from the glycocalyx and the substrate. PLoS Comput Biol. 2009; 5:e1000604. [PubMed: 20011123]
9. Hansma P, Yu H, Schultz D, et al. The tissue diagnostic instrument. Rev Sci Instrum. 2009; 80:6.
10. Sinkus R, Tanter M, Xydeas T, Catheline S, Bercoff J, Fink M. Viscoelastic shear properties of in vivo breast lesions measured by MR elastography. Magn Reson Imaging. 2005; 23:159–165. [PubMed: 15833607]
11. Thomas A, Degenhardt F, Farrokh A, Wojcinski S, Slowinski T, Fischer T. Significant differentiation of focal breast lesions: calculation of strain ratio in breast sonoelastography. Acad Radiol. 2010; 17:558–563. [PubMed: 20171905]
12. Partridge SC, Rahbar H, Murthy R, et al. Improved diagnostic accuracy of breast MRI through combined apparent diffusion coefficients and dynamic contrast-enhanced kinetics. Magnetic Resonance in Medicine. 2011; 65:1759–1767. [PubMed: 21254208]
13. Sharma U, Danishad KKA, Seenu V, Jagannathan NR. Longitudinal study of the assessment by MRI and diffusion-weighted imaging of tumor response in patients with locally advanced breast cancer undergoing neoadjuvant chemotherapy. NMR Biomed. 2009; 22:104–113. [PubMed: 18384182]

14. Singer L, Wilmes LJ, Saritas EU, et al. High-resolution diffusion-weighted magnetic resonance imaging in patients with locally advanced breast cancer. Acad Radiol. 2012; 19:526–534. [PubMed: 22197382]

15. Saritas EU, Cunningham CH, Lee JH, Han ET, Nishimura DG. DWI of the spinal cord with reduced FOV single-shot EPI. Magnet Reson Med. 2008; 60:468–473.

16. Klifa, C.; Carballido-Gamio, J.; Wilmes, L., et al. Quantification of breast tissue index from MR data using fuzzy clustering. 26th Annual International Conference of the IEEE Engineering in Medicine and Biology Society, IEMBS; 2004. p. 1667-1670.

17. Klifa, C.; Newitt, D.; Park, C., et al. Digital proximity mapping to assess radial dependence of breast stromal enhancement associated with response to neoadjuvant chemotherapy. 19th Annual Meeting of ISMRM; Montreal. 2011. p. abstract 1023

18. Hylton NM. Vascularity assessment of breast lesions with gadolinium-enhanced MR imaging. Magn Reson Imaging Clin N Am. 1999; 7:411–420. [PubMed: 10382170]

19. Fangberget A, Nilsen LB, Hole KH, et al. Neoadjuvant chemotherapy in breast cancer-response evaluation and prediction of response to treatment using dynamic contrast-enhanced and diffusion-weighted MR imaging. Eur Radiol. 2011; 21:1188–1199. [PubMed: 21127880]

20. Conklin MW, Eickhoff JC, Riching KM, et al. Aligned collagen is a prognostic signature for survival in human breast carcinoma. Am J Pathol. 2011; 178:1221–1232. [PubMed: 21356373]

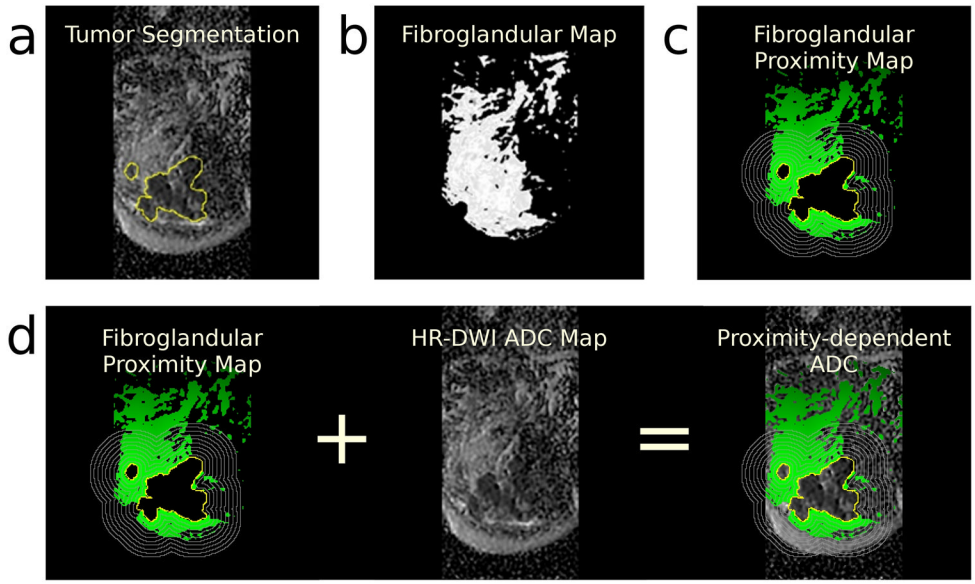

Figure 1.
The proximity mapping method takes the difference of the segmentation of tumor (a) and fibroglandular map (b) to create a fibroglandular proximity map (c). The fibroglandular proximity map can then be applied to any registered functional image to calculate proximity-dependent values. In this study, the fibroglandular proximity map was applied to HR-DWI ADC images (d)

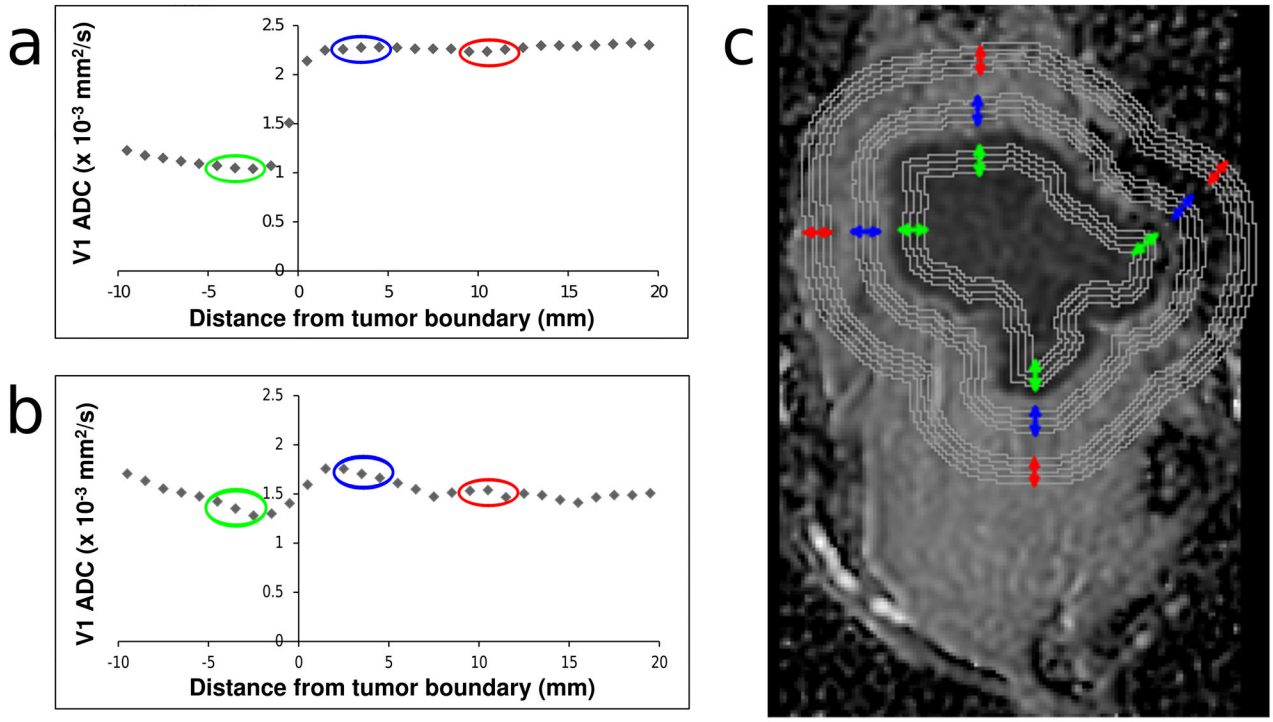

Figure 2.

The ADC plotted as a function of distance from the tumor boundary for two patients at visit 1 (a, b). The distance ranges of ADC_{inner}, ADC_{prox}, and ADC_{dist} are circled in green, blue, and red, respectively. A slice of a representative proximity-dependent ADC map (Patient 1) is shown with arrows corresponding to ADC_{inner}, ADC_{prox}, and ADC_{dist} at visit 1 (c)

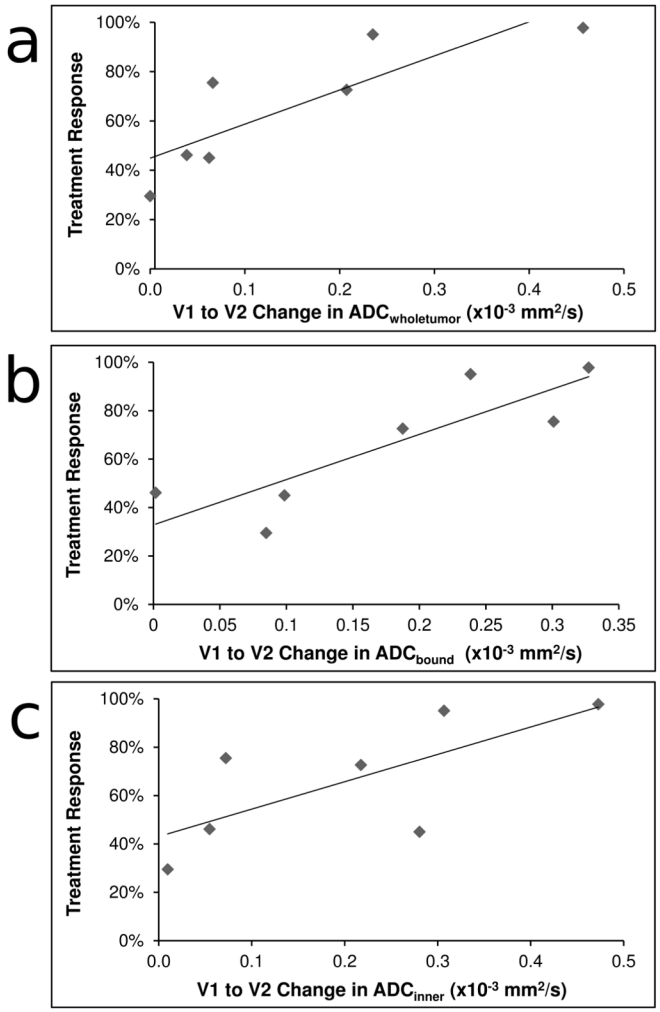

Figure 3.
The visit 1 (V1) to visit 2 (V2) change in $ADC_{wholetumor}$ (a), ADC_{bound} (b), and ADC_{inner} (c) is plotted versus the treatment response

Table 1

Apparent diffusion coefficient (ADC) measurements for seven patients at visit 1 (V1) and visit 2 (V2)

		ADC_{inner}	ADC_{prox}	ADC_{dist}	$ADC_{wholetumor}$
Patient 1	**Visit 1**	1.009 ± 0.450	1.207 ± 0.517	1.301 ± 0.524	0.955 ± 0.488
	Visit 2	1.081 ± 0.522	1.448 ± 0.541	1.495 ± 0.553	1.016 ± 0.563
Patient 2	**Visit 1**	1.701 ± 0.479	2.379 ± 0.512	2.245 ± 0.456	1.719 ± 0.475
	Visit 2	1.919 ± 0.413	2.459 ± 0.413	2.262 ± 0.378	1.921 ± 0.411
Patient 3	**Visit 1**	1.054 ± 0.225	2.272 ± 0.324	2.250 ± 0.335	1.159 ± 0.257
	Visit 2	1.108 ± 0.269	2.174 ± 0.344	2.131 ± 0.395	1.193 ± 0.302
Patient 4	**Visit 1**	1.278 ± 0.484	2.013 ± 0.555	2.007 ± 0.513	1.416 ± 0.577
	Visit 2	1.559 ± 0.507	2.008 ± 0.508	1.920 ± 0.455	1.473 ± 0.497
Patient 5	**Visit 1**	1.446 ± 0.384	2.043 ± 0.611	2.080 ± 0.707	1.434 ± 0.413
	Visit 2	1.919 ± 0.428	2.105 ± 0.539	2.140 ± 0.634	1.886 ± 0.440
Patient 6	**Visit 1**	1.544 ± 0.451	2.016 ± 0.380	2.163 ± 0.490	1.551 ± 0.408
	Visit 2	1.554 ± 0.451	2.035 ± 0.433	2.113 ± 0.543	1.546 ± 0.410
Patient 7	**Visit 1**	1.351 ± 0.276	1.707 ± 0.592	1.511 ± 0.629	1.443 ± 0.304
	Visit 2	1.658 ± 0.239	1.602 ± 0.407	1.641 ± 0.458	1.673 ± 0.269

The units for all values are $\times 10^{-3}$ mm^2/s. ADC_{inner}, ADC_{prox}, ADC_{dist}, and $ADC_{wholetumor}$ are ADC values for the region: −5 to −2 mm, 2 to 5 mm, 9 to 13 mm, and $-\infty$ to 0 mm, respectively.

Table 2

The Spearman rank correlations between treatment response and visit 1 (V1) to visit 2 (V2) change in the regional apparent diffusion coefficient (ADC) measurements

	Region	ρ	95% CI	p value
$\mathbf{ADC_{prox}}$	2 to 5	0.143	−0.684 to 0.809	0.76
$\mathbf{ADC_{dist}}$	9 to 13	0.714	−0.084 to 0.954	0.07
$\mathbf{ADC_{inner}}$	−5 to −2	0.750	−0.007 to 0.961	0.05
$\mathbf{ADC_{wholetumor}}$	$-\infty$ to 0	0.929	0.584 to 0.990	0.003
$\mathbf{ADC_{bound}}$	−2 to 2	0.857	0.294 to 0.979	0.01

Each ADC variable represents the respective region indicated. ρ is the estimated Spearman correlation. 95% CI indicates the 95% confidence interval.